

Resonant excitation of graphene K-phonon and intra-Landau level excitons in magneto-optical spectroscopy.

M. Orlita*,^{1,2} Liang Z. Tan,³ M. Potemski,¹ M. Sprinkle,⁴ C. Berger,^{4,5} W. A. de Heer,⁴ Steven G. Louie*,³ and G. Martinez¹

¹*Laboratoire National des Champs Magnétiques Intenses, CNRS-UJF-UPS-INSA, B.P. 166, 38042 Grenoble Cedex 9, France*

²*Institute of Physics, Charles University, Ke Karlovu 5, CZ-121 16 Praha 2, Czech Republic*

³*Department of Physics, University of California at Berkeley, and Materials Sciences Division, Lawrence Berkeley National Laboratory, Berkeley, CA 94720*

⁴*School of Physics, Georgia Institute of Technology, Atlanta, Georgia 30332, USA*

⁵*Institut Néel, CNRS-UJF B.P. 166, 38042 Grenoble Cedex 9, France*

(Dated: January 24, 2022)

Precise infra-red magneto-transmission experiments have been performed in magnetic fields up to 32 T on a series of multi-layer epitaxial graphene samples. We observe changes in the spectral features and broadening of the main cyclotron transition when the incoming photon energy is in resonance with the lowest Landau level separation and the energy of a K point optical phonon. We have developed a theory that explains and quantitatively reproduces the frequency and magnetic field dependence of the phenomenon as the absorption of a photon together with the simultaneous creation of an intervalley, intra-Landau level exciton and a K -phonon.

Phonons, electrons, holes and plasmons are fundamental elementary excitations in solids, and their interactions among themselves and with light strongly influence the electronic and optical properties of a system. Graphene, a single atomic layer of carbon, exhibits many fascinating properties of basic and practical interest. Its low-energy charge carriers behave like two-dimensional (2D) massless Dirac fermions. The unique electronic structure of graphene has led to the prediction and observation of a number of novel phenomena involving various multi-elementary excitation interactions including electron-photon, electron-phonon, electron-electron, and electron-plasmon couplings. Recent discoveries include the observation of plasmarens in ARPES [1], controlling of quantum pathways in inelastic light scattering [2], and strong excitonic effects in optical absorption [3–5], among others.

In this paper, we report the discovery of another intriguing phenomenon seen in the magneto-optical response of graphene when the incoming photon energy is in resonance with the lowest Landau level separation and the energy of a Brillouin-zone-boundary phonon at the K point. The frequency and magnetic field dependence of the spectral features are understood and explained in terms of resonant transitions which involve the absorption of a photon together with the simultaneous creation of an intervalley, intra-Landau level exciton and a K -phonon. The phenomenon provides a novel manifestation of multi-elementary excitation interactions in condensed matter.

The phonons that interact the most strongly with electrons in graphene are those at the Brillouin-zone-center (Γ) and at the Brillouin-zone-boundary (K) [6]. The Γ -phonon has been the subject of theoretical study [6] and its signatures have been observed in several

experiments[7, 8]. The K -phonon also interacts strongly with electrons, giving rise to characteristic features in Raman spectra [8]. Compared to Γ -phonons, the effect of K -phonons on optical experiments is more subtle and indirect, due to the large difference in momenta between photons and the K -phonons. The large wavevector of the K -phonons may also couple the two inequivalent valleys in the graphene band structure, introducing an additional degree of freedom into the system. The present study shows that this valley degree of freedom in the coupling has unique and important consequences in the magneto-optical response of graphene.

In our experiment, precise infra-red transmission measurements were performed on multi-layer epitaxial graphene samples, at 1.8 K, under magnetic fields up to 32 T. It is known that under a perpendicular magnetic field B , the electronic structure of graphene is quantized to discrete Landau levels (LL) with the energy $E_n = \text{sgn}(n)v_F\sqrt{2e\hbar B|n|}$ where n are integers including 0. Multiple optical transitions are allowed and have been observed [9] between LL $|n|$ to $|n| \pm 1$ if these levels have appropriate occupation factors. We focus our attention on the magnetic field evolution of the transmission spectrum near the main optical absorption peak, with energy $E_{01} = v_F\sqrt{2e\hbar B}$ involving the $n = 0$ LL (i.e., transitions from $n = -1$ to $n = 0$ or from $n = 0$ to $n = 1$.) It is discovered that a strong change in the optical spectrum occurs when E_{01} reaches an energy near the energy of a K -phonon. This is interpreted as a signature of a new multi-elementary excitation phenomenon involving interaction between electrons and the K -phonon, and a theory is developed to explain quantitatively the phenomenon.

A series of four multi-layer epitaxial graphene samples were grown [10] on the C-terminated surface of SiC. The thickness of the SiC substrate has been reduced

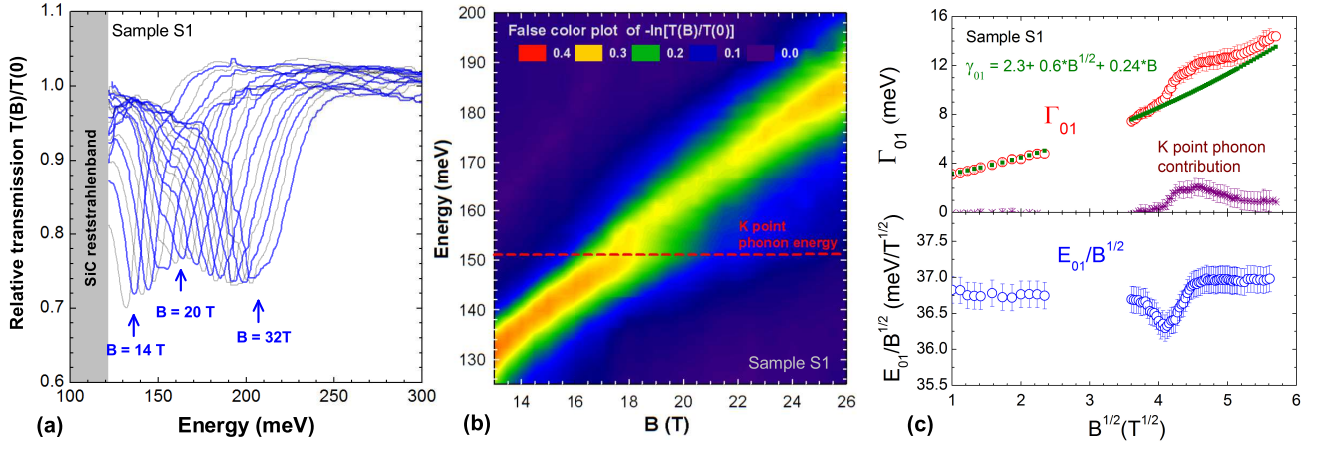


FIG. 1: (a) Relative transmission spectra ($T(B)/T(0)$) of sample S1, for different magnetic field values. (b) Same data as in (a) presented in a false color plot of $-\ln[T(B)/T(0)]$. (c) Bottom panel: variation of cyclotron transition energy $E_{01}/B^{1/2}$ as a function of $B^{1/2}$ (open blue circles). Top panel: variation of the fitted linewidth $\Gamma_{10}(B)$ of the transition $E_{01}(B)$ as a function of $B^{1/2}$ (open red circles). This variation is de-convoluted in two parts, one named $\gamma_{01}(B)$ (green dots) and the remaining part (stars) which is assigned to the K -phonon contribution.

to $60\mu\text{m}$ in order to minimize the very strong double-phonon absorption of SiC in the energy range of interest. Whereas the transmission spectra reveal some contributions of graphite Bernal-stacked inclusions, the major part displays the electronic band structure of an isolated graphene monolayer resulting from the characteristic rotational stacking of the sheets [11]. Using standard techniques [12], we measure the relative transmission spectra $\text{TR}(B, \omega)$ (see Supplementary Information SI-I).

The TR spectra of the sample S1 are displayed in Fig. 1a and b for different values of B . They show, as for all samples, an apparent splitting of the transmission dip into two and a pronounced increase of the broadening of the dip, as well as a change in the B -field dependence of the overall position E_{01} for fields larger than 17 T.

In general, the detailed analysis of such spectra requires the use of a multi-layer dielectric model including all layer dielectric properties of the sample. In particular, for each graphene sheet, one has to introduce the corresponding components of the optical conductivity tensor $\sigma_{xx}(\omega)$ and $\sigma_{xy}(\omega)$, defined by $J_\alpha = \sum_\beta \sigma_{\alpha\beta} \mathcal{E}_\beta$ (J_α and \mathcal{E}_β denote current density and electric field vectors respectively). Here, the x and y -axis lie in the plane of the sample. For instance $\sigma_{xx}(\omega)$, for transitions involving the $n=0$ LL, is written as:

$$\sigma_{xx}(\omega, B) = i \frac{e^3 B}{\hbar \omega} \sum_{r,s} \frac{M_{r,s}^2 (f_r(B) - f_s(B))}{\hbar \omega - E_{r,s}(B) + i\Gamma_{rs}(B)} \quad (1)$$

where r, s scan the values 0 and ± 1 , $0 \leq f_r \leq 1$ is the occupation factor of the LL r , $M_{r,s}$ the optical matrix element, $E_{r,s} = E_r - E_s = E_{01}$ and $\Gamma_{rs}(B) = \Gamma_{01}(B)$ measures the broadening of the transition. However this approach requires the knowledge of the number of effec-

tive active layers as well as their carrier densities which, in turn, implies some approximations (see SI-II for details). We will use this approach *in a refined analysis*, but in our initial analysis, fit directly the E_{01} transition with a single Lorentzian line.

This fit provides, for each value of B , two independent parameters $E_{01}(B)$ and $\Gamma_{01}(B)$ which are plotted in Fig. 1c as a function of $B^{1/2}$. The variation of $\Gamma_{01}(B)$ shows clearly an extra bump beyond 17 T (clearly apparent in Fig. 1b) whereas that of $E_{01}(B)/B^{1/2}$ exhibits a downwards kink at the same field. The evolution of $\Gamma_{01}(B)$ is decomposed in two parts: one named $\gamma_{01}(\text{meV}) = 2.3 + 0.6\sqrt{B} + 0.24B$ (full dots) and an extra contribution to Γ_{01} represented by stars in the top panel of Fig. 1c. The same decomposition is obtained for all samples with slightly different coefficients which are discussed in SI-II. The \sqrt{B} dependence of γ_{01} is attributed to scattering with short range impurities [14]; the linear variation with B is not predicted by scattering mechanisms considered in previous studies [14] and will be discussed later. The shape of the extra contribution to Γ_{01} has a threshold at around 17 T (~ 151 meV) with a maximum amplitude of about 2 meV for all samples, within the experimental uncertainties, before decreasing at higher fields. In that energy range the only likely excitations in graphene which could play a role are the zone-boundary K -phonons [15, 16]. Note that, at this threshold energy, the evolution $E_{01}/B^{1/2}$ (bottom panel of Fig. 1c) is the signature of interactions because, in the absence of such interactions, it should be an horizontal line. This is reminiscent of the response function of the Fröhlich interaction observed in polar semiconductors [12, 13] where a zone-center longitudinal optical phonon is emitted when the energy of the cyclotron transition

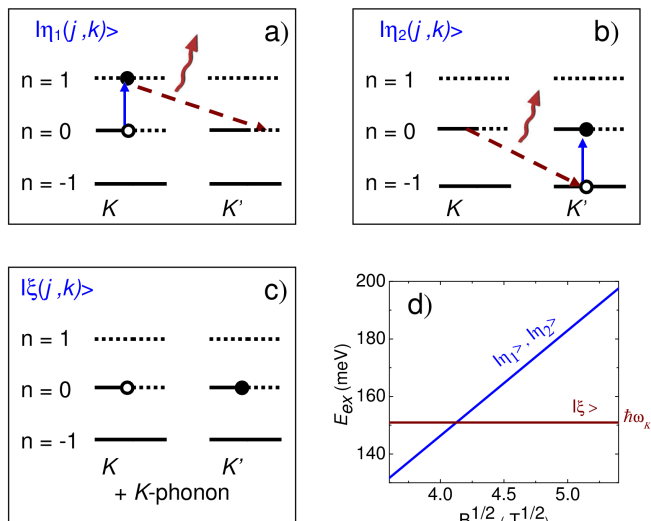


FIG. 2: Cyclotron resonant excitations $|\eta_1(j, k)\rangle$ (a) and $|\eta_2(j, k)\rangle$ (b) involving the $n = 0$ Landau levels, at either the K or K' valley, with the excitation energy $E_{ex} = E_{01}$. (c) Excited state $|\xi_{\vec{q}}(j, k)\rangle$ corresponding to intervalley transfer of an electron within the $n = 0$ LL from \vec{K} to \vec{K}' and creation of a phonon with wavevector $\vec{K} + \vec{q}$, which has excitation energy $E_{ex} = \hbar\omega_{\vec{K}+\vec{q}}$. (d) At resonance, i.e. $E_{01} = \hbar\omega_{\vec{K}+\vec{q}}$, $|\eta_1\rangle$ and $|\eta_2\rangle$ may be transformed to $|\xi\rangle$ via an emission of a $\vec{K} + \vec{q}$ phonon as indicated by the dashed brown lines. The mixing between the three excited states, mediated by the electron-phonon interaction, is the strongest when the resonance condition is satisfied ($E_{01} = \hbar\omega_{\vec{K}+\vec{q}}$). Electron-phonon scatterings involving LL $|n| \geq 2$ do not result in similar resonances in the experimental energy range (see SI-IV.) In general, there are scattering processes involving phonons of different \vec{q} vectors near K , but we find the coupling strength significant only in a small region with $\vec{q} \approx 0$ where the phonon energy is essentially constant and equal to $\hbar\omega_K$. The theoretical description of this continuum of near K phonons may be incorporated effectively by considering a single state $|\xi\rangle$ with a complex self energy and using an appropriately renormalized coupling constant between $|\eta_1\rangle$, $|\eta_2\rangle$ and $|\xi\rangle$ (see derivation in SI-IV).

exceeds that of the phonon. However, graphene is not a polar material and, furthermore, we are not expecting a direct interaction of the K -phonon with the infra-red light. One therefore has to explain why and how the K -phonons enter the interaction.

The mechanism for the interaction of the cyclotron transition with the K -phonon is not *a priori* clear for the reason of conservation of wavevector, i.e., a state corresponding to an optical cyclotron transition which has wavevector 0 cannot decay into a state with a phonon of wavevector \vec{K} without simultaneously emitting another entity of wavevector $-\vec{K}$. Given that this interaction must necessarily involve the electron-phonon interaction, and that the low-energy electronic states at the two valleys of graphene are separated in reciprocal space by a wavevector \vec{K} , we propose that an intervalley intra-

LL electron scattering process (creation of a zero-energy intervalley electron-hole pair) is responsible for the observed phenomenon (Fig. 2.)

To explain the observed spectral features, we shall consider the coupling of the photo-excited (cyclotron transition) states (denoted as $|\eta_1(j, k)\rangle$ and $|\eta_2(j, k)\rangle$ for the $0 \rightarrow 1$ and $-1 \rightarrow 0$ LL transitions respectively) with an excited state of the system containing an intervalley, intra-Landau level electron-hole pair excitation and a K -phonon of wavevector $\vec{K} + \vec{q}$ (denoted as $|\xi_{\vec{q}}(j, k)\rangle$). See Fig. 2. Here j is the valley index and k is the quantum number which describes the degenerate states within a LL. As illustrated in Fig. 2, at cyclotron transition energy E_{01} near $\hbar\omega_{\vec{K}+\vec{q}}$, $|\eta_1(j, k)\rangle$ and $|\eta_2(j, k)\rangle$ are connected to $|\xi_{\vec{q}}(j, k)\rangle$ via an emission of $\vec{K} + \vec{q}$ phonons. The electron-phonon coupling in the system can then strongly mix these states at resonance and lead to significant changes in the absorption spectrum.

In order to reproduce quantitatively the transmission spectra, one has now to use the multi-layer dielectric model (see SI-II for details). The optical conductivity is calculated using the Green's function formalism introduced by Toyozawa [18]. The conductivity components are

$$\text{Re } \sigma_{ij}(\hbar\omega) \propto \text{Im}\langle 0|M_i G(\hbar\omega)M_j|0\rangle \quad (2)$$

where $|0\rangle$ is the ground state of the system, and M_i , M_j are row and column vectors containing optical matrix elements. G is the retarded Green's function written here as $G(\hbar\omega) = [\hbar\omega - H - \Sigma(\omega) + is]^{-1}$ with $s \rightarrow 0^-$ with H being a 3x3 Hamiltonian describing the interaction between the three states $|\eta_1\rangle$, $|\eta_2\rangle$ and $|\xi\rangle$. The poles of G are broadened by a self energy $\Sigma(\omega)$ reflecting additional lifetime effects due to the K -phonon dispersion and the excitations from electron-acoustic phonons scattering, electron-electron interactions and other environmental effects not captured by H (see SI-V). In the theoretical calculations, we have incorporated this additional physics near resonance with a broadening function of the form $\Gamma_{01}(\omega, B) = \gamma_{01}(B) + \text{Im}(\Sigma(\omega))$ with $\gamma_{01}(B)$ given above and $\text{Im}(\Sigma)$ taken to be $\text{Im}(\Sigma(\omega)) = \pi A^2 f(R/\hbar\omega_K)\theta(\hbar\omega - \hbar\omega_K)e^{-R(\omega/\omega_K - 1)}$. The derivation of the form of $\text{Im}(\Sigma(\omega))$ within our theoretical model is given in SI-IV and SI-V. A^2 (meV²) = 1.94 × B (T) is the electron-phonon parameter determined from Ref. [16]. f is a factor, dependent on the relative magnitudes of the valley (Δ_V) and spin (Δ_S) splittings of the $n = 0$ LL, that is determined by the occupations of the spin and valley sublevels of the $n = 0$ LL (see SI-IV). The threshold structure of $\text{Im}(\Sigma(\omega))$ represents the onset of K -phonon emission at energies above $\hbar\omega_K$. The only parameters in the theory are the phonon energy $\hbar\omega_K$ and the factor R . The absorption spectra can be obtained from $\text{Re } \sigma(\omega)$ by a simple proportionality relation (see SI-V and [9]).

In Fig. 3 we compare the experimental data, for sample S1, with the calculated results from the model with

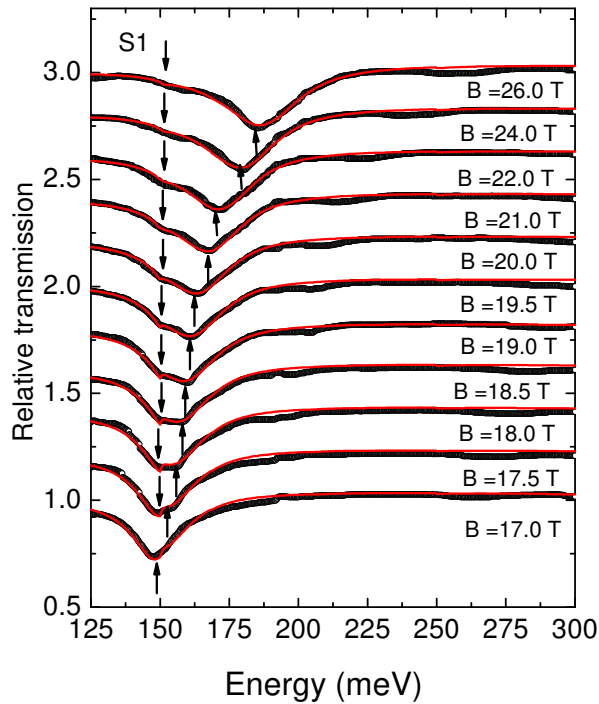


FIG. 3: Comparison, for different values of the magnetic field, of experimental data for sample S1 (open black dots) with the theoretical curves (red lines) using the proposed K-phonon interaction model. As a guide for the eye, upward arrows show the evolution of the main cyclotron resonance line whereas downward arrows point the structure corresponding to the emission of K -phonons.

$\Delta_V > \Delta_S$. We have taken $\hbar\omega_K = 151$ meV and $R = 3$. The Fermi velocity $v_{F01} = 1.012 \times 10^6$ ms $^{-1}$ for the transitions between the $n = 0$ LL and $n = \pm 1$ LL has been determined experimentally from the positions of the cyclotron transition lines (see SI-II and SI-III). The same parameters have been used for all the graphene samples (see SI-III). The good agreement between theory and experiment, for all samples, lends strong support to the physical mechanism proposed for the phenomenon. It is, however only obtained when assuming $\Delta_V > \Delta_S$ (Fig. 4).

An interpretation of the linear term in $\gamma_{01}(B)$ is that it may be a broadening resulting from the breaking of the valley degeneracy (Fig. 4), consistent with the prediction that $\Delta_V \propto B$, according to several theoretical models [20–22]. In this picture, the values of E_{01} at the two valleys differ by Δ_V [23], resulting in a broadening of the main line by a similar amount. An inspection of the linear term in $\gamma_{01}(B)$ shows that it is greater than the value of Δ_S due to Zeeman splitting. This is consistent with our conclusion that $\Delta_V > \Delta_S$ in our samples (Fig. 4). However, further investigations are needed to test if the valley splitting is indeed the main contributor to the linear term in γ_{01} .

To conclude, we have observed splitting of spectral fea-

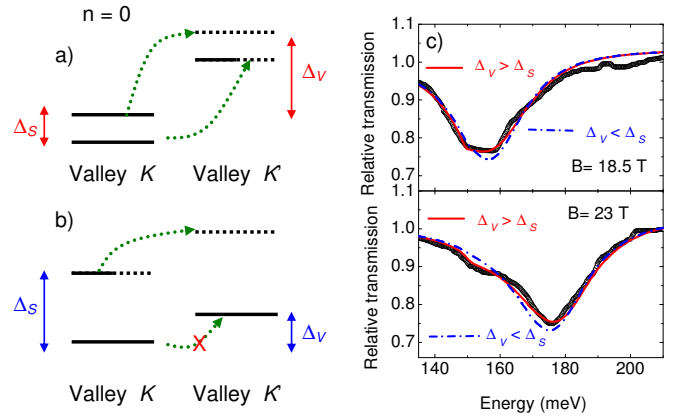


FIG. 4: (a), (b) The spin and valley sublevels of the $n = 0$ LL, for the case when $\Delta_V > \Delta_S$ and $\Delta_V < \Delta_S$ respectively. In the former case, intervalley electronic transitions are possible for both spin orientations. In the latter case, only one spin orientation supports intervalley electronic transitions, owing to the Fermi factor. The effective coupling strength is therefore different in the two cases giving rise to different predictions for the transmission spectra. (c) A comparison between experimental spectra and theoretical simulations for $\Delta_V > \Delta_S$ and $\Delta_V < \Delta_S$ for values of magnetic field $B = 18.5$ T and $B = 23.0$ T respectively. For all our samples the splitting of the valley degeneracy is larger than the spin splitting. This is consistent with recent tunnelling spectroscopy experiments on graphene on SiC [19]. Theoretical discussions on the relative magnitudes of these splittings can be found in Refs. [20–25].

tures and broadening of the main absorption line above 17 T in our infra-red transmission experiments on epitaxial graphene that we attribute to a resonance between cyclotron transitions and K-phonon emission coupled with a zero-energy intervalley electron-hole excitation. We have developed a theoretical model that reproduces the experimental results with quantitative agreement, thereby shedding light on the nature of the optical transitions and electron-phonon interaction in graphene under strong magnetic fields. Our results indicate that the valley splitting of the LL is larger than the spin splitting in our samples. To our knowledge, this is the first instance where information on the sublevel structure of graphene has been obtained using infra-red transmission measurements, complementing transport- [26, 27] and tunnelling-based [19] experiments.

We thank Cheol-Hwan Park for useful discussions. L.Z.T. and the theoretical analysis were supported by the Director, Office of Science, Office of Basic Energy Sciences, Materials Sciences and Engineering Division, U.S. Department of Energy under Contract No. DE-AC02-05CH11231. Numerical simulations were supported in part by NSF Grant DMR10-1006184. Computational resources were provided by NSF through TeraGrid resources at NICS and by DOE at Lawrence Berkeley National Laboratory’s NERSC facility. This work has been supported in part by by EuroMagNET II under EU

Contract No. 228043. This work has also been supported by projects GACR P204/10/1020, GRA/10/E006 (Eurographene-EPIGRAT) and IRMA.

-
- [1] A. Bostwick *et al.*, Science **328**, 999-1002 (2010).
 [2] C.-F. Chen *et al.*, Nature **471**, 617-620 (2011).
 [3] L. Yang *et al.*, Phys. Rev. Lett. **103**, 186802 (2009).
 [4] V. G. Kravets *et al.*, Phys. Rev. B **81**, 155413 (2010).
 [5] K. F. Mak, J. Shan and T. F. Heinz, Phys. Rev. Lett. **106**, 046401 (2011).
 [6] H. Suzuura and T. Ando, J. Phys. Soc. Jpn. , **77**, 044703 (2008).
 [7] A. Bostwick *et al.*, Nature physics **3**, 36-40 (2007).
 [8] A. C. Ferrari *et al.*, Phys. Rev. Lett. **97**, 187401 (2006).
 [9] M. L. Sadowski *et al.*, Phys. Rev. Lett. **97**, 266405 (2006).
 [10] C. Berger *et al.*, J. Phys. Chem. B **108**, 19912-19916 (2004)
 [11] J. Hass *et al.*, Phys. Rev. Lett. **100**, 125504 (2008).
 [12] C. Faugeras *et al.*, Phys. Rev. B **80**, 073303 (2009).
 [13] M. Orlita *et al.*, Euro. Phys. Lett. **92**, 37002 (2010).
 [14] C. H. Yang, F. M. Peeters and W. Xu, Phys. Rev. B **82**, 075401 (2010). *ibid*, Phys. Rev. B **82**, 205428 (2010).
 [15] J. Maultzsch, S. Reich, C. Thomsen, H. Requardt and P. Ordejón, Phys. Rev. Lett. **92**, 075501 (2004).
 [16] A. Grüneis *et al.*, Phys. Rev. B **80**, 085423 (2009).
 [17] U. Fano, Phys. Rev. **124**, 1866-1878 (1961).
 [18] Y. Toyozawa *et al.*, J. Phys. Soc. Jpn. **22** 1337-1349 (1967).
 [19] Y. Song *et al.*, Nature **467**, 185-189 (2010).
 [20] K. Nomura and A. MacDonald, Phys. Rev. Lett. **96**, 256602 (2006).
 [21] J. Alicea and M. Fisher, Phys. Rev. B **74**, 075422 (2006).
 [22] K. Yang, S. Das Sarma and A. MacDonald, Phys. Rev. B **74**, 075423 (2006).
 [23] J.-N. Fuchs and P. Lederer, Phys. Rev. Lett. **98**, 016803 (2007).
 [24] M. O. Goerbig, R. Moessner and B. Doucot, Phys. Rev. B **74**, 161407 (2006)
 [25] D. Abanin, P. Lee and L. Levitov, Phys. Rev. Lett. **98**, 156801 (2007).
 [26] K. Bolotin *et al.*, Nature **462**, 196-199 (2009)
 [27] X. Du *et al.*, Nature **462**, 192-195 (2009).

Supplementary information for Resonant excitation of graphene
K-phonon and intra-Landau level excitons in magneto-optical
spectroscopy.

M. Orlita*,^{1,2} Liang Z. Tan,³ M. Potemski,¹ M. Sprinkle,⁴ C.
Berger,^{4,5} W. A. de Heer,⁴ Steven G. Louie*,³ and G. Martinez¹

¹*Laboratoire National des Champs Magnétiques Intenses,
CNRS-UJF-UPS-INSA, B.P. 166, 38042 Grenoble Cedex 9, France*

²*Institute of Physics, Charles University,
Ke Karlovu 5, CZ-121 16 Praha 2, Czech Republic*

³*Department of Physics, University of California
at Berkeley, and Materials Sciences Division,*

Lawrence Berkeley National Laboratory, Berkeley, CA 94720

⁴*School of Physics, Georgia Institute of Technology, Atlanta, Georgia 30332, USA*

⁵*Institut Néel, CNRS-UJF B.P. 166, 38042 Grenoble Cedex 9, France*

(Dated: January 24, 2022)

I. EXPERIMENTAL DETAILS

Far infra-red magneto-optical experiments have been performed at magnetic field strengths up to 29-32 T and at a fixed temperature of 1.8 K. The light (provided and analyzed by a Fourier transform spectrometer) was delivered to the sample by means of light-pipe optics. All experiments were performed with nonpolarized light, in the Faraday geometry with the wave vector of the incoming light parallel to the magnetic field direction and perpendicular to the plane of the samples. A Si bolometer was placed directly beneath the sample to detect the transmitted radiation. The response of this bolometer is strongly dependent on the magnetic field. Therefore, in order to measure the absolute transmission $TA(B, \omega)$, we used a sample-rotating holder and measure for each value of B a reference spectrum through a hole. These spectra are normalized in turn with respect to $TA(0, \omega)$ to obtain a relative transmission spectrum $TR(B, \omega)$ which only displays the magnetic field dependent features. Those spectra are presented in Fig. 1.

II. GLOBAL ANALYSIS OF THE SPECTRA

In Fig. 1, the relative transmission spectra are shown for sample S2 (a), sample S3 (b) and sample S4 (c). In general, for filling factors $\nu < 2$, the oscillator strength of a magneto-optical transition in graphene is expected to be proportional to \sqrt{B} if the broadening parameter Γ_{01} is a constant. If $\Gamma_{01} \sim \sqrt{B}$ the minimum of the transmission should be independent on B . However and as for the sample S1 (Fig. 1(a) of the main text), all the observed transmission data display an extra broadening of the E_{01} transition for magnetic fields values larger than 17 T. This leads us to conclude that such an effect is an intrinsic property of the graphene sheets.

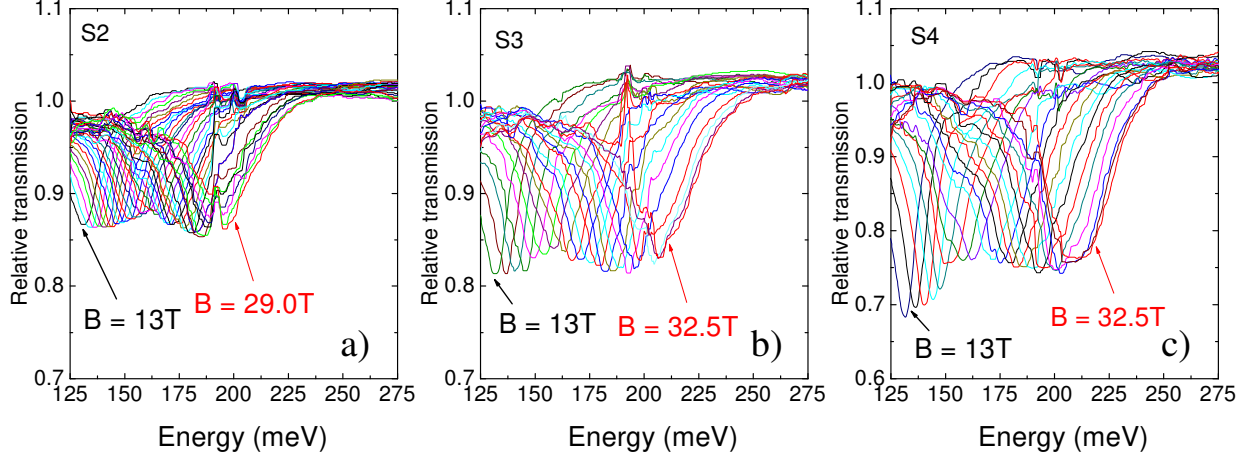


FIG. 1. Relative transmission spectra, as a function of the energy, for different values of the magnetic field B : (a) sample S2, (b) sample S3 and (c) Sample S4.

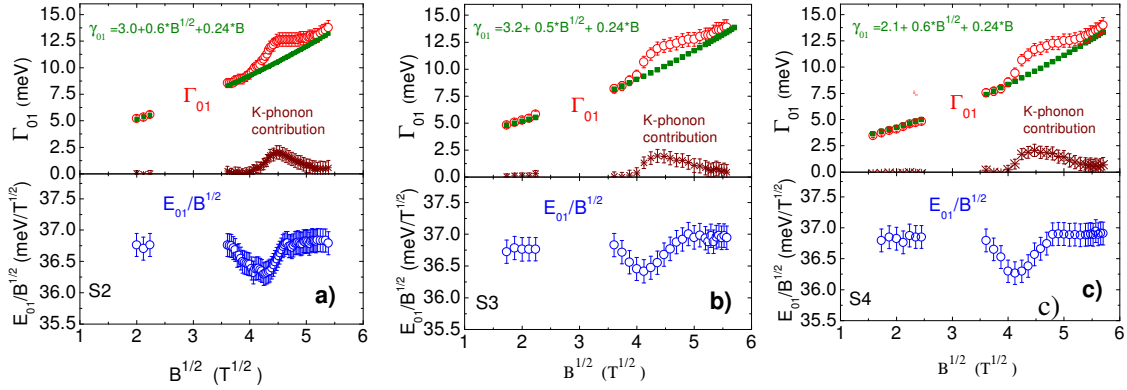


FIG. 2. Bottom panels: variation of E_{01}/\sqrt{B} as a function of \sqrt{B} (open blue circles). Top panels: variation of the fitted linewidth $\Gamma_{10}(B)$ of the transition $E_{01}(B)$ as a function of \sqrt{B} (open red circles). This variation is decomposed in two parts, one named $\gamma_{01}(B)$ (green dots) and the remaining part (wine stars) which will be assigned to the K -phonon contribution. (a) sample S2, (b) sample S3 and (c) sample S4.

One can, as said in the main paper, analyze globally the E_{01} transition by a fit with a single Lorentzian line which provides the evolution of the two parameters $E_{01}(B)$ and $\Gamma_{01}(B)$ as a function of $B^{1/2}$ as displayed in Fig. 2 for samples S2, S3 and S4. However, as this will be

explained in the following, the model for the electron- K -phonon interaction is dependent on the filling factor ν of the graphene layer and therefore on its carrier density N_s ($\nu = N_s\Phi_0/B$, Φ_0 being the flux quantum). We have therefore used a multi-layer dielectric model to analyze the data. This model assumes that each graphene sheet is uniformly spread over the sample. This is a strong assumption, difficult to justify *a priori* but which is necessary here to get some relative quantitative information. If one knows, for a given sample, the number N_{eff} of effective layers and their carrier densities, one can fit quantitatively the data using Eq.1 of the main text when v_0 , the Fermi velocity entering the optical matrix element ($M_{r,s} \propto v_0$), is known. Very often the value v_0 is taken identical to the Fermi velocity v_F deduced from the magnetic field dependence of the optical transitions. However v_F is the re-normalized velocity including electron-electron interactions and it has been shown [1] that v_0 should be the band velocity ignoring these interactions as given, for instance, by LDA calculations. In the present work, we have taken for all samples $v_0 = 0.85 \times 10^6 m/sec$. We next evaluate the number N_{eff} for each sample. In the range of magnetic fields 13 to 17 T, the relative transmission spectra (Fig. 1) reaches values above 1 which depends on the number N_{eff} : we have therefore a guide to estimate this quantity. This is however only a guide because this value is also sensitive to the effective coverage of each layer over the sample and, of course, to experimental uncertainties. We estimate $N_{eff} = 3$ for sample S2, $N_{eff} = 5$ for sample S3 and $N_{eff} = 6$ for samples S1 and S4. The carrier density N_s for each layer is determined in the following way: one knows that, for $2 < \nu < 6$, upon increasing B , the intensity of the E_{01} absorption starts to increase, at the expense of the intensity of the E_{12} transition ($E_{12} = E_2 - E_1$). The intensity does not change with B for $\nu < 2$. Therefore, the disappearance of the optical transition E_{12} corresponds to $\nu = 2$. Following step by step, as a function of B , the transmission spectra one can evaluate the carrier density N_{sm} for

each layer m . This is a loop process which converges reasonably (within 20 per cent) but has to be done independently for each sample. This gives reliable values for the uppermost layers which are the less doped and will play a major role when the electron- K -phonon interaction will be switched on. The value of N_{s1} for the layer close to the SiC substrate can be set arbitrary to 5 to 6 $10^{12}cm^{-2}$ as given by transport data on samples grown under similar conditions: this layer indeed does not contribute to the transition E_{01} in the present experiment. Fitting the data with such a multi-layer dielectric model and using Eq.1 of the main text provides also the two parameters $E_{01}(B)$ and $\Gamma_{01}(B)$: it turns out that within the experimental errors (error bars in Fig. 2) they are identical to the results obtained previously by fitting the data with a single Lorentzian line. Therefore these results are quite robust.

We note that, for all samples, the variation of $\Gamma_{01}(B)$ as a function of \sqrt{B} (top panels of Fig. 2) displays with respect to a smooth variation, an extra bump. We have decomposed this variation into two parts, $\gamma_{01}(B)$ which is quadratic in \sqrt{B} and an extra contribution displayed by stars in the top panels of Fig. 2. We will assign this latter contribution to the K -phonon interaction contribution. We have taken for $\gamma_{10}(B)$ a quadratic dependence of the form: $\gamma_{01}(B) = \gamma_0 + \gamma_1 \times \sqrt{B} + \gamma_2 \times B$. Though it is possible to fit $\Gamma_{01}(B)$ for B lower than 16 T with $\gamma_2 = 0$, the resulting decomposition gives, for the K -phonon contribution, a variation which does not decrease at high fields (or high energies) which is not physical. We are then lead to introduce this B -dependence which, in turn, will determine the way the interaction decreases at high energies. This is of course dependent of the model used to describe the interaction as discussed in section V-B. We have used the same parameter $\gamma_2 = 0.24$ for all samples which in turn gives a value for $\gamma_1 = 0.55 \pm 0.05$ (the error bars covering the coefficients for all samples). This dependence on B is not explained by existing scattering mechanisms [2]. Coming back to the K -phonon interaction contribution, we find,

for all samples a similar variation: after a threshold around 17 T, it reaches a maximum of $2.1 \pm 0.1 meV$ (the error bars covering the values found for all samples).

In the bottom panels of Fig. 2 (and Fig 1b of the main paper), the variation of $E_{01}/B^{1/2}$ versus $B^{1/2}$ is displayed. These variations show a downward kink at a value of B corresponding to the onset of the K -phonon contribution. It is important to note that, within the experimental errors, the K -phonon contribution to $\Gamma_{01}(B)$ and the variation of $E_{01}/B^{1/2}$, plotted as a function of the energy are indeed Kramers-Krönig related.

Though the present analysis did not focus on the higher energy transitions, we have fit as well over a large energy range the transitions between the $n = -2$ to $n = 1$ and $n = -1$ to $n = 2$ Landau levels corresponding to the energy $\epsilon_{-1,2} = \epsilon_{-2,1} = v_F \sqrt{2e\hbar B} \times (\sqrt{2} + 1)$. For all samples this transition can be fitted with $v_F = 1.025 \times 10^6 \text{ms}^{-1}$. It is interesting to note that the width of these transitions $\Gamma_{-12}(B)$ is found to vary linearly as a function of $B^{1/2}$ like $\Gamma_{-12}(B) = \eta_0 + \eta_1 \times \sqrt{B}$ without, within the experimental errors, a significant contribution proportional to B . Therefore it seems that the dependence on B adopted for $\gamma_{01}(B)$ is specific of the $n = 0$ LL.

III. FITTING THE EXPERIMENTAL TRANSMISSION CURVES

Up to this point the treatment of the transmission curves has been done assuming that all optically active layers have the same broadening parameter $\Gamma_{10}(B)$. In reality the variation of $E_{01}/B^{1/2}$ displayed in the bottom panels of Fig. 2 lead us to conclude that this K -phonon interaction, reminiscent of the Fröhlich interaction observed in polar semiconductors [3, 4], has to be treated as a function of the energy. In other words, for each layer simulated with Eq.1 of the main text, the denominator $\hbar\omega - E_{01}(B) + i\Gamma_{01}(B)$ has to be replaced by $\hbar\omega - \epsilon_{01}(B) + i\gamma_{01}(B) + \Sigma(\omega, B)$. Therefore the new pole occurs at an energy $\epsilon_{01}(B) -$

$Re(\Sigma(\omega, B))$ with a width $\gamma_{01}(B) + Im(\Sigma(\omega, B))$. Here $\Sigma(\omega, B)$ is the self energy of the phonon interaction and $\epsilon_{01}(B) = v_F\sqrt{2e\hbar B}$ the non re-normalized value of the transition energy. The model for treating the self energy will be detailed in section V: the imaginary part of the self energy depends on a parameter R (see Eq.17), the phonon energy $\hbar\omega_K$ and an amplitude squared A^2 governing the electron-phonon interaction (see section V-B). For each sample we have used the background broadening parameter $\gamma_{01}(B)$ as obtained from the preceding fitting (which is sample dependent) but the parameters for the phonon-interaction are the same for all samples: $R = 3$, $\hbar\omega_K = 151$ meV and $A^2 = 1.94$ meV² $\times B$. The same Fermi velocity $v_F = 1.012 \times 10^6$ ms⁻¹ has been taken for all samples to describe the transition $\epsilon_{01}(B)$. It is a little bit smaller than the value found for the transition $\epsilon_{-12}(B)$ which may be a sign of electron-electron interactions [1].

The results from the model, presented in the next sections, are compared to the experimental data in Fig. 3. Including the experimental errors, the parameter R is determined within 15 per cent. However the fitting is done assuming that the valley splitting Δ_V is larger than the spin splitting Δ_S , a result which is clearly beyond the experimental uncertainties as evidenced by the comparison of both simulations with the experimental spectra (see Fig.4 of the main text). As a matter of fact, our model predicts, see section IV-B, that the K -phonon interaction should vanish when the filling factor ν goes to zero if $\Delta_V < \Delta_S$.

Despite the different approximations made to treat the spectra, we obtain a fit of transmission curves which is acceptable with the same basic parameters (v_0 , v_F , R , $\hbar\omega_K$, A^2) for all samples. This makes us confident in the basic physical picture and the process we have adopted to treat these spectra.

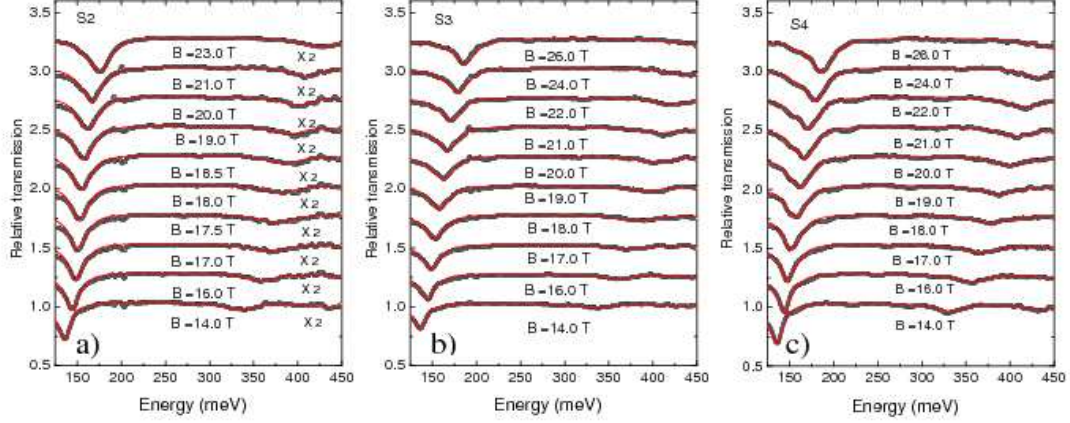


FIG. 3. Comparison of experimental data (open black dots) with the simulated traces (red lines) using the proposed K-phonon interaction model for different values of the magnetic field. Theoretical spectra (from SI-IV) were calculated with parameters described in the text. (a) sample S2 (scale multiplied by 2), (b) sample S3 and (c) sample S4.

IV. DERIVATION OF THE MODEL HAMILTONIAN

A. Electron-phonon interaction

Expressions for the electron- K -phonon interaction in graphene in the plane wave basis can be found in Ref.[5]. After performing a change of basis to the Landau level (LL) basis, the electron-phonon interaction can be written as:

$$H^{e-ph} = \sum_{\substack{jnn' \\ kk'\vec{q}}} g_{kk'\vec{q}}^{jnn'} c_{j+1,n',k'}^\dagger c_{j,n,k} (a_{j,\vec{q}}^\dagger + a_{j,\vec{q}}). \quad (1)$$

Here, $c_{j,n,k}^\dagger$ is the electron creation operator in valley $j = 0, 1$ (corresponding to the K or K' valley), for the LL n and wavevector k in the Landau gauge, and $a_{j,\vec{q}}^\dagger$ is the K or K' phonon creation operator of wavevector \vec{q} relative to the K or K' point. The addition of the valley index $j + 1$ is understood to be modulo 2. The matrix elements are:

$$g_{kk'\vec{q}}^{jnn'} = \frac{2\beta\gamma}{b^2} \sqrt{\frac{\hbar}{2N_c M \omega_K}} C i e^{2\pi i/3} \delta_{k,k'+q_x} e^{iq_y(k-q_x/2)l_B^2} (J_{|n'|-1,|n|-1}(\vec{q}) - \text{sgn}(n)\text{sgn}(n')J_{|n'|,|n|}(\vec{q})) \quad (2)$$

with

$$J_{n',n}(\vec{q}) = \left(\frac{n'!}{n!}\right)^{1/2} e^{-q^2 l_B^2/4} \left(\frac{q_x l_B + i q_y l_B}{2}\right)^{n'-n} L_n^{n'-n} \left(\frac{q^2 l_B^2}{2}\right) \quad \text{when } n' \geq n \geq 0$$

$$J_{n',-1}(\vec{q}) = 0 \quad (3)$$

$$J_{n',n}(\vec{q}) = J_{n,n'}^*(-\vec{q})$$

In these equations, $b = a/\sqrt{3}$ is the C-C bond length, $a = 2.46 \text{ \AA}$ is the lattice period, $\gamma = \sqrt{3}at_0/2$, and $t_0 = 2.7 \text{ eV}$ is the nearest neighbor hopping parameter. $\beta = -(b/\gamma)(d\gamma/db)$ is a dimensionless coupling parameter. N_c is the number of unit cells, M is the mass of a carbon atom, ω_K is the K -phonon frequency and $l_B = \sqrt{\hbar/(eB)}$ is the magnetic length. The constant C takes the value of $1/2$ if $|n| > 0$ and $|n'| > 0$, and $1/\sqrt{2}$ otherwise. $L_m^n(u)$ denotes the Laguerre polynomial and $\text{sgn}(n) = 1$ when $n \geq 1$ and $\text{sgn}(n) = -1$ otherwise.

B. Choice of reduced Hilbert space

The cyclotron transitions of interest are (see Fig. 2 of main text):

$$|\eta_1(j, k)\rangle = c_{j,1,k}^\dagger c_{j,0,k}|0\rangle \quad (4)$$

$$|\eta_2(j, k)\rangle = c_{j,0,k}^\dagger c_{j,-1,k}|0\rangle.$$

Here, $|0\rangle$ is the ground state. We now consider candidate states $|\xi\rangle$ to be included in the model, such that the experimental spectra could be explained by their interactions with the cyclotron transition states. Such states have to satisfy two conditions: (i) they can couple

directly to $|\eta_1\rangle, |\eta_2\rangle$ via the electron-phonon interaction Eq. 1 (i.e. $\langle\xi|H^{e-ph}|\eta_{1,2}\rangle \neq 0$), and (ii) in order to describe the resonance at $E = \hbar\omega_K$ the states $|\xi\rangle$ must have energy $\langle\xi|H|\xi\rangle \approx \hbar\omega_K$.

Based on the form of the electron-phonon interaction, it is evident that $|\xi\rangle$ must contain a K -phonon as well as intervalley electronic transitions. Condition (ii) implies that these transitions must be between LL of the same LL index because the electronic part of $|\xi\rangle$ must have the same energy as $|0\rangle$. We therefore consider the states

$$|\xi_{\vec{q}}(j, k)\rangle = c_{j+1,0,k-q_x}^\dagger c_{j,0,k} a_{j,\vec{q}}^\dagger |0\rangle. \quad (5)$$

Note that the single phonon states $a_{j,\vec{q}}^\dagger |0\rangle$ satisfy condition (ii) but not condition (i). In Eq. 5, the inter-valley transitions are between the $n = 0$ LL because this is the only partially empty LL in the experiment.

Another class of states that can couple to the cyclotron transition states is $\{b^\dagger|\xi_{\vec{q}}(j, k)\rangle, b^\dagger b^\dagger|\xi_{\vec{q}}(j, k)\rangle, \dots\}$, which contain one or more acoustic phonons in addition to $|\xi_{\vec{q}}(j, k)\rangle$. Here, b^\dagger, b^\dagger create acoustic phonons.

C. Integration over the phonon continuum

Because of the dispersion of optical phonons at the K point [6], and the coupling to acoustic phonons, the energies of the states that can couple to $|\eta_1\rangle, |\eta_2\rangle$ form a continuum, bounded below by ω_K . In this section, we perform an integration over this continuum. We start with a Hamiltonian of a general form that describes two degenerate states interacting with a continuum of states. For a given (j, k) ,

$$H_1 = \begin{pmatrix} E_{01} & 0 & u_1(\omega_K, \omega_K) & u_1(\omega_K + \delta, \omega_K) & u_1(\omega_K + 2\delta, \omega_K) & \dots \\ 0 & E_{01} & u_2(\omega_K, \omega_K) & u_2(\omega_K + \delta, \omega_K) & u_2(\omega_K + 2\delta, \omega_K) & \dots \\ u_1(\omega_K, \omega_K) & u_2(\omega_K, \omega_K) & \omega_K & v & v & \dots \\ u_1(\omega_K + \delta, \omega_K) & u_2(\omega_K + \delta, \omega_K) & v & \omega_K + \delta & v & \dots \\ u_1(\omega_K + 2\delta, \omega_K) & u_2(\omega_K + 2\delta, \omega_K) & v & v & \omega_K + 2\delta & \dots \\ \vdots & \vdots & \vdots & \vdots & \vdots & \ddots \end{pmatrix}. \quad (6)$$

The first two columns (rows) represent the cyclotron transition states $|\eta_1\rangle$, $|\eta_2\rangle$. The rest of the columns (rows) represent the continuum of states that contain phonons. Here, $\delta > 0$ is a small positive energy. The function $u_i(\omega, \omega_K)$ (may be obtained from Eqs. 1, 2) describes the interaction between $|\eta_i\rangle$ and a $|\xi\rangle$ state of the continuum of energy ω , while v describes the interaction within the continuum.

We now treat the problem in two successive approximations. The first one assumes that the phonons have no dispersion, which allows us to introduce an effective coupling constant V and work in a restricted Hilbert space having effectively one phonon. The second assumption takes into account the dispersion of phonons as a correction to the first approximation. This is done by introducing a self energy term in the Green's function (see next section for the treatment of the Green's function).

An effective Hamiltonian in our restricted Hilbert space for dispersion-less phonons can be written as:

$$H = \begin{pmatrix} E_{01} & 0 & V_1 \\ 0 & E_{01} & V_2 \\ V_1^* & V_2^* & \omega_K \end{pmatrix} \quad (7)$$

where the values of V_1 and V_2 are chosen such that H and H_1 have the same eigenvalues when $\delta = 0$. We have found that $V_1 = -V_2 = V = \sqrt{\sum_{\vec{q}}' g_{1\vec{q}} g_{1\vec{q}}^*}$ (see below for explicit expressions of this parameter.)

We then introduce the effects of the phonon continuum using second-order Löwdin perturbation theory [7]. This is done by introducing a self energy $\Sigma_{ph}(\omega)$ in our Green's function treatment of the optical response functions in the restricted Hilbert space of H [8]. The condition imposed by the model is that the Green's functions $(\omega - H - \Sigma_{ph}(\omega) - i0^+)^{-1}$ and $(\omega - H_1 - i0^+)^{-1}$ are equal in the space spanned by $|\eta_1\rangle, |\eta_2\rangle$. Explicit expressions for the different components of $\Sigma_j(\omega)$ are given in the next section.

In the definition of the parameter V , the prime ($'$) on the sum indicates that not all \vec{q} vectors have to be summed over, because only a fraction $0 < f < 1$ of the total number of $|\xi_{\vec{q}}\rangle$ states are available, depending on the filling factor. Then,

$$V = \sqrt{\sum_{\vec{q}}' g_{1\vec{q}} g_{1\vec{q}}^*} = \sqrt{f \sum_{\text{all } \vec{q}} g_{1\vec{q}} g_{1\vec{q}}^*} = A\sqrt{f} \quad (8)$$

The constant $A^2 = \sum_{\text{all } \vec{q}} g_{1\vec{q}} g_{1\vec{q}}^* = \frac{9\sqrt{3}\beta^2\gamma^2 B}{4\pi a^2 M\omega_K}$ can be obtained from Eq. 2. In reality this has to be corrected by the introduction of electron-electron interactions [6]. To obtain the value of f , we examine the occupation numbers of the $n = 0$ LL of the K and K' valleys.

Let us define ν to be the filling factor, including spin and orbital degeneracies. For example, $\nu = 0$ at charge neutrality and $\nu = 2$ if the carrier concentration is such that the LL $n = 0$ is fully occupied. For the case of $\Delta_V > \Delta_S$, filling factor $\nu < 1$ (Fig. 4a), we

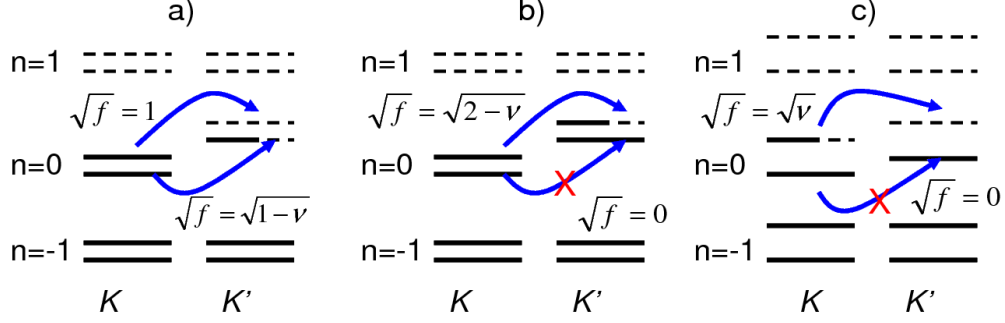


FIG. 4. a) Schematic diagram of the Landau levels when $\Delta_V > \Delta_S$ and $\nu < 1$; b) Schematic diagram of the Landau levels when $\Delta_V > \Delta_S$ and $1 < \nu < 2$ and c) Schematic diagram of the Landau levels when $\Delta_V < \Delta_S$ and $\nu < 1$.

have $\sqrt{f} = 1$ for the spin up transitions, and $\sqrt{f} = \sqrt{1-\nu}$ for the spin down transitions. Whereas for $\Delta_V > \Delta_S$, filling factor $1 < \nu < 2$ (Fig. 4b), we have $\sqrt{f} = \sqrt{2-\nu}$ for the spin up transitions, and $\sqrt{f} = 0$ for the spin down transitions.

On the other hand, if $\Delta_V < \Delta_S$, the expressions are the same as the case of $\Delta_V < \Delta_S$ when the filling factor is $1 < \nu < 2$, but when $\nu < 1$: we have $\sqrt{f} = \sqrt{\nu}$ for the spin up transitions, and $\sqrt{f} = 0$ for the spin down transitions (Fig. 4c). Therefore, in that case, for undoped graphene layer, the interaction disappears.

V. EVALUATION OF OPTICAL CONDUCTIVITY

A. Green function formalism

The Green function formalism for the optical conductivity $\text{Re } \sigma_{ij} \sim \text{Im } \langle 0 | M_i^\dagger G M_j | 0 \rangle$ has been introduced in the main text. Here, we provide some explicit expressions for the form of the optical conductivity. In order to facilitate the discussion of the self energy $\Sigma_{ph}(\omega)$, we express the Green's function matrix in the basis of eigenstates of the model Hamiltonian H

(Eq. 7).

$$G' = \begin{pmatrix} G'_{11} & 0 & 0 \\ 0 & G'_{22} & 0 \\ 0 & 0 & G'_{33} \end{pmatrix}, \quad G'_{jj} = \frac{1}{\omega - \varepsilon_j - is}, \quad s = 0^+ \quad (9)$$

The primed (') quantities are expressed in the basis of the eigenstates of H . The eigenvalues ε_j of the Hamiltonian H (Eq. 7) are

$$\begin{aligned} \varepsilon_1 &= E_{01} \\ \varepsilon_{2,3} &= \frac{1}{2} \left(E_{01} + \hbar\omega_K \pm \sqrt{(E_{01} - \hbar\omega_K)^2 + 8V^2} \right) \end{aligned} \quad (10)$$

The Green's function matrix (G) in the original basis (i.e., the same basis as Eq. 7) can be recovered by a unitary transformation $G = UG'U^{-1}$.

$$U = \begin{pmatrix} \frac{1}{\sqrt{2}} & \frac{-V}{\sqrt{2V^2+(E_{01}-\varepsilon_2)^2}} & \frac{-V}{\sqrt{2V^2+(E_{01}-\varepsilon_3)^2}} \\ \frac{1}{\sqrt{2}} & \frac{V}{\sqrt{2V^2+(E_{01}-\varepsilon_2)^2}} & \frac{V}{\sqrt{2V^2+(E_{01}-\varepsilon_3)^2}} \\ 0 & \frac{E_{01}-\varepsilon_2}{\sqrt{2V^2+(E_{01}-\varepsilon_2)^2}} & \frac{E_{01}-\varepsilon_3}{\sqrt{2V^2+(E_{01}-\varepsilon_3)^2}} \end{pmatrix} \quad (11)$$

Then, for instance, the σ_{xx} component of the optical conductivity is related to $\langle 0|M_x^\dagger GM_x|0\rangle = \langle 0|M_x^\dagger UG'U^{-1}M_x|0\rangle$, where $M_x^\dagger = (M_{1x}, M_{2x}, 0)$ is a row vector containing the optical matrix elements.

B. Discussion of Σ_{ph}

We introduce self energy terms into the diagonal elements of G'

$$G'_{jj} = \frac{1}{\omega - \varepsilon_j - i0^+} \rightarrow \frac{1}{\omega - \varepsilon_j - \Sigma_j(\omega)} \quad (12)$$

From second-order Löwdin perturbation theory (see previous section), we have found

$$\begin{aligned}
\text{Im } \Sigma_1 &= 0 \\
\text{Im } \Sigma_2 &= \Sigma(\omega, \omega_K) \\
\text{Im } \Sigma_3 &= \Sigma(\omega, \omega_K)
\end{aligned} \tag{13}$$

where the imaginary part of the self energy has the form

$$\text{Im } \Sigma(\omega) = \theta(\omega - \omega_K)(u(\omega, \omega_K))^2 \tag{14}$$

Here, $u(\omega, \omega_K) = |u_1(\omega, \omega_K)| = |u_2(\omega, \omega_K)|$. In the basis of Eq. 7, the Green's function can be written as

$$G = \begin{pmatrix} G_{11} & G_{12} & G_{13} \\ G_{21} & G_{22} & G_{23} \\ G_{31} & G_{32} & G_{33} \end{pmatrix} \tag{15}$$

$$\begin{aligned}
G_{11} = G_{22} &= \frac{1}{2} \left(\frac{1}{\omega - E_{01} - i0^+} + \frac{1}{\omega - E_{01} - i0^+ - \Sigma(\omega)} \right) \\
G_{12} &= -\frac{1}{2} \left(-\frac{1}{\omega - E_{01} - i0^+} + \frac{1}{\omega - E_{01} - i0^+ - \Sigma(\omega)} \right).
\end{aligned} \tag{16}$$

$\text{Im } \Sigma(\omega)$ has a threshold at ω_K that arises irrespective of the form of the coupling matrix element u . In this model, the threshold is always located at the lower bound of the energies of the continuum of states. We have chosen, motivated by the experimental data (see top panels of Fig. 2), for u^2 the form

$$(u(\omega, \omega_K))^2 = D \exp(-R(\omega/\omega_K - 1)) \tag{17}$$

Using the sum rule for $\text{Im}(G)$ together with the constraint that H_1 must reduce to H in the limit where $R \rightarrow \infty$ (the limit where the continuum collapses to a single energy

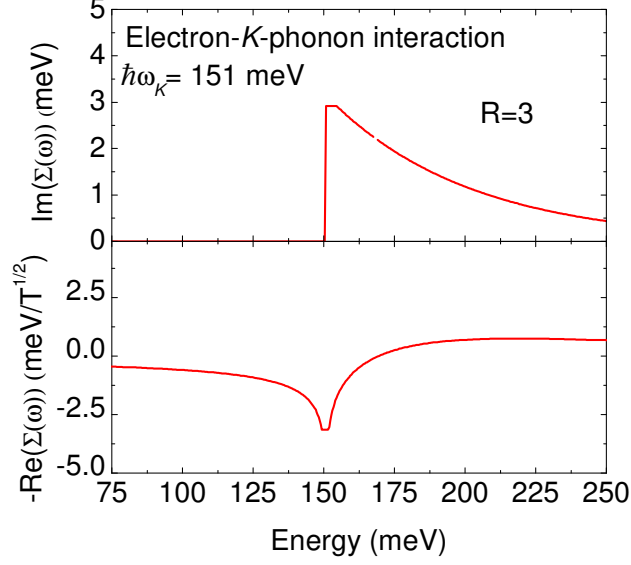


FIG. 5. Top panel: Imaginary part of the self-energy (Σ_2 or Σ_3 in Eq. 13) with $\nu = 0$. Bottom panel: Real part of the self-energy with $\nu = 0$ as deduced from Kramers-Kronig transformation of the Imaginary part. The behavior of the real part of the self-energy, as a function of energy, is quite similar to that of $E_{01}/B^{1/2}$ when adding the contribution of the non re-normalized value of the transition energy $\epsilon_{01}(B)/\sqrt{B} = v_F\sqrt{2e\hbar} = 36.8\text{meV}/T^{1/2}$. (See bottom panels of Fig. 2 and Fig.1b of the main text.)

ω_K), the value of D can be fixed at $D = (\pi R V^2)/(\hbar\omega_K)$. The model is not sensitive to the exact functional form of Eq. 14 as long as the qualitative features such as the exponential decay and the presence of a threshold at $\omega = \omega_K$ are preserved. We then have two independent parameters to describe the interaction, V^2 and R . As derived in Eq. 8, $V^2 = A^2 f$ and we will use the value $A^2(\text{meV}^2) = 1.94 \times B(\text{T})$ [6]. The energy range of $u(\omega, \omega_K)$ contains contribution from the K -phonon dispersion and multi-acoustic phonon processes. The only remaining fitting parameter is R . In the interpretation of the continuum as states containing multiple acoustic phonons, the exponential factor in Eq. 17 describes the decreasing probability of multiple acoustic phonon emission far from the threshold energy.

With this simplified model, and knowing the experimental results, we have chosen the value $R = 3$ as sketched in Fig. 5 which in turn is coherent with the value of the linear B term used for $\gamma_{01}(B)$. This also gives reasonable values for $\text{Re}\Sigma(\omega)$ (bottom panel Fig. 5) as compared to the experimental values. Of course the extension in energy corresponding to this R value is quite high but it does not play a role in the actual fitting process limited to about 200 meV (see Fig. 3). Though, within the experimental errors, the fit of data is acceptable with $R = 3$, it could be also accepted for R values, as well as the γ_2 values of $\gamma_{01}(B)$ differing by 15 per cent. Knowing that the spin splitting $\Delta_S/B \simeq 0.12 - 0.15$ meV/T and that the introduction of $\Delta_V \propto B$ should result in an extra broadening of the E_{01} transition, the introduction of the γ_2 -term is explained naturally by the fact that it should be larger than Δ_S/B .

We note finally that the introduction of the interference term G_{12} (Eq.16) (which corresponds to interference effects between the cyclotron transitions at the two valleys) is essential to reproduce the experimental results.



- [1] Yu. Bychkov and G. Martinez, Phys. Rev. B **77**, 125417 (2008).
- [2] C. H. Yang, F. M. Peeters and W. Xu, Phys. Rev. B **82**, 075401 (2010); *ibid*, Phys. Rev. B **82**, 205428 (2010).
- [3] C. Faugeras *et al.*, Phys. Rev. B **80**, 073303 (2009).
- [4] M. Orlita *et al.*, Euro. Phys. Lett. **92**, 37002 (2010).
- [5] H. Suzuura and T. Ando, J. Phys. Soc. Jpn. **77**, 044703 (2008).
- [6] A. Grüneis *et al.*, Phys. Rev. B **80**, 085423 (2009).
- [7] P.-O. Löwdin, J. Chem. Phys. **19** 1396 (1951).

[8] Y. Toyozawa *et al.*, J. Phys. Soc. Jpn. **22** 1337-1349 (1967).